Radiative carrier lifetime in $Ge_{1-x}Sn_x$ midinfrared emitters

Gérard Daligou, Anis Attiaoui, Simone Assali, Patrick Del Vecchio, and Oussama Moutanabbir*

Department of Engineering Physics, École Polytechnique de Montréal, C.P. 6079, Succ. Centre-Ville, Montréal, Québec H3C 3A7, Canada

(Received 19 February 2023; revised 18 September 2023; accepted 20 September 2023; published 1 December 2023)

$Ge_{1-x}Sn_x$ semiconductors have promise for large-scale, monolithic, midinfrared photonics and optoelectronics. However, despite the successful demonstration of several $Ge_{1-x}Sn_x$-based photodetectors and emitters, key fundamental properties of this material system are yet to be fully explored and understood. In particular, little is known about the role of the material properties in controlling the recombination mechanisms and their consequences for the carrier lifetime. Evaluating the latter is in fact fraught with large uncertainties that are exacerbated by the difficulty in investigating narrow-band-gap semiconductors. To alleviate these limitations, herein we demonstrate that the behavior of the radiative carrier lifetime can be evaluated from straightforward excitation power- and temperature-dependent photoluminescence measurements. To this end, a theoretical framework is introduced to simulate the measured spectra by combining the band structure calculations from the *k.p* theory and the envelope function approximation to estimate the absorption and spontaneous emission. The model computes explicitly the momentum matrix element to estimate the strength of the optical transitions in single bulk materials, unlike the joint density of states model that assumes a constant matrix element. Based on this model, the temperature-dependent emission from $Ge_{0.83}Sn_{0.17}$ samples at a biaxial compressive strain of −1.3% is investigated. The simulated spectra reproduce accurately the measured data thereby enabling the evaluation of the steady-state radiative carrier lifetimes, which are found in the range 3–22 ns for temperatures between 10 and 300 K at an excitation power of 0.9 kW/cm^2. For a lower power of 0.07 kW/cm^2, the obtained lifetime has a value of 1.9 ns at 4 K. The demonstrated approach yielding the radiative lifetime from simple emission spectra will provide valuable inputs to improve the design and modeling of $Ge_{1-x}Sn_x$-based devices.

DOI: 10.1103/PhysRevApplied.20.064001

I. INTRODUCTION

$Ge_{1-x}Sn_x$ alloys constitute an emerging class of group IV semiconductors providing a tunable narrow band gap, which have been highly attractive to implement scalable, silicon-compatible, midinfrared photonic and optoelectronic devices [1]. This potential becomes increasingly significant with the progress in nonequilibrium growth processes enabling high-Sn-content $Ge_{1-x}Sn_x$ layers and heterostructures leading to the demonstration of a variety of monolithic midinfrared emitters and detectors [2–18]. Notwithstanding the recent developments in device engineering, the impact of structural characteristics on the basic behavior of charge carriers is yet to be fully understood. This includes the role of Sn content, lattice strain, and growth defects in shaping the nature and magnitude of the recombination mechanisms and their consequences for the carrier lifetime. Particularly, investigating the latter remains a daunting task due to the lack of methods and tools that can be applied to probe charge carriers in narrow-band-gap materials. For instance, time-resolved photoluminescence (PL) can with difficulty be applied to investigate materials at emission wavelengths in the midinfrared range as high-speed detectors covering this range are not broadly available. Thus, the very few reported time-resolved studies concern $Ge_{1-x}Sn_x$ emitting below 2.3 μm corresponding to a relatively low Sn content and/or highly compressively strained materials [19–21].

In an attempt to circumvent the aforementioned limitations, a recent study employed time-resolved PL with a nonlinear crystal allowing the up-conversion of photons emitted to a shorter wavelength that can be detected by a conventional silicon-based avalanche photodiode [19]. An effective carrier lifetime of 217 ps at 20 K was estimated for $Ge_{0.875}Sn_{0.125}$ with −0.55% strain using this method [19]. Additionally, by investigating spin-dependent optical transitions leveraging the Hanle effect under steady-state excitation, systematic studies combining modeling and magneto-PL analysis of pseudomorphic layers at a Sn content below 10% reported a radiative lifetime in the range 19–48 ns and an effective lifetime in the range 0.5–2.5 ns at 10 K [20]. However, significantly higher effective carrier lifetimes reaching 450 ns were recently reported for $Ge_{1-x}Sn_x$ ($x < 0.06$) grown on In-Al-As buffer layers

*oussama.moutanabbir@polymtl.ca

as measured by contactless microwave photoconductive decay [21]. This scarcity of studies on carrier dynamics in narrow-band-gap $Ge_{1-x}Sn_x$ semiconductors limits the understanding of their fundamental behavior and hinders the development of accurate and predictive models for $Ge_{1-x}Sn_x$-based midinfrared optoelectronic devices.

In this work, we demonstrate that straightforward PL analyses along with an appropriate theoretical framework are sufficient to alleviate these challenges and extract the radiative carrier lifetime in $Ge_{1-x}Sn_x$ midinfrared emitters and evaluate its evolution as a function of temperature. The approach relies on the simulation of the experimental PL spectra by combining band structure calculations using the *k.p* formalism together with the envelope function approximation (EFA) to estimate the absorption and spontaneous emission spectra. Unlike the joint density of states (JDOS) model, in which the momentum matrix element is considered constant, the oscillator strengths are explicitly computed in this model.

In the following sections, the model is described followed by an experimental demonstration using as-grown $Ge_{0.83}Sn_{0.17}$ layers, emitting at wavelengths above 3 μm. Note that the presented approach is only applicable to direct-band-gap semiconductors for which the nonradiative recombinations are negligible.

II. THEORETICAL FRAMEWORK

The PL spectrum intensity is usually determined using the direct interband emission theory and the spontaneous emission spectrum [22]. Indeed, by considering a slab of homogeneously excited material, Lasher and Stern [23] and Würfel [24] expressed the *external* flux of spontaneous radiative emission in terms of the spectral absorptivity under nonequilibrium conditions in terms of the quasi-Fermi level splitting, $\Delta\mu = \mu_e - \mu_h$. The resulting "Lasher-Stern-Würfel" (LSW) equation is

$$I_{\mathrm{PL}}(E) = \frac{2\pi}{\hbar^3 c^2}\frac{E^2 a(E)}{\exp(\frac{E-\Delta\mu}{k_B T}) - 1} = \frac{a(E)}{\alpha(E)}\frac{r^{\mathrm{sp}}(E)}{4n_r^2}, \quad (1)$$

where r^{sp} is the *internal* spontaneous emission spectrum, $\alpha(E)$ is the absorption spectrum, and n_r is the refractive index of the medium. $a(E)$ is the spectral absorptivity defined as expression (2) with R the reflection from the outside onto the sample surface and d the thickness of the conceptual slab [25]:

$$a(E) = (1 - R(E))\Big[1 - \exp(-\alpha(E)d)\Big]. \quad (2)$$

Note that d is also considered a characteristic length scale over which carriers are generated, travel, and recombine radiatively [25]. Based on this definition, this parameter should be inversely proportional to the absorption coefficient at the excitation wavelength, i.e., $d \approx 1/\alpha(\lambda_{\mathrm{laser}})$. However, the PL spectrum will mostly be centered around the band-gap energy where $\alpha(E)$ is at least 1 or 2 orders of magnitude smaller than $\alpha(\lambda_{\mathrm{laser}})$ in the case of nonresonant excitation. Therefore $\alpha d << 1$ and the absorbance is $a(E) \approx A\alpha(E)$. In that case, the PL intensity from Eq. (1) becomes

$$I_{\mathrm{PL}}(E) \approx \frac{2\pi A}{\hbar^3 c^2}\frac{E^2\alpha(E)}{\exp(\frac{E-\Delta\mu}{k_B T}) - 1} \approx \frac{A}{4n_r^2} r^{\mathrm{sp}}(E). \quad (3)$$

With this approximation, the PL spectrum intensity is entirely defined by either the internal spontaneous emission spectrum or the absorption spectrum, depending on the formula used.

The spontaneous emission spectrum r^{sp} is calculated using Fermi's golden rule [26,27]. In the current literature, the computation of the spontaneous emission spectrum is done using band structures extracted from the empirical pseudopotential method [28–30], tight-binding model [31], multibands *k.p* formalism [32,33], and the parabolic band approximation (PBA) [34,35].

For direct-band-gap semiconductors, where the optoelectronics interactions relevant to the PL happen relatively close to the band edges, the multibands *k.p* formalism and the PBA are the most suitable approaches.

For the analysis of the experimental PL spectra of single direct-band-gap semiconductors, r^{sp} is commonly computed using the JDOS model [34,36–39]. This model relies on the PBA, which leads to a set of relatively simple analytical formulas. It is most accurate for a nondegenerately doped semiconductor in a weak-injection regime with the quasi-Fermi levels lying within the band gap and away from the different band edges by several $k_B T$. This model was extended in Ref. [40] to account for different excitation regimes by explicitly evaluating the quasi-Fermi level splitting $\Delta\mu$, and the nonequilibrium absorption spectrum in Eq. (3). However, it still relies on the PBA, which restricts the analysis. Indeed, for higher excitation power and/or doping concentration, μ_e and μ_h would shift towards, and even beyond, the band edges where the PBA should be less accurate. Besides, for a biaxially strained semiconductor, the $\vec{k}$ direction degeneracies in the Brillouin zone (BZ) are expected to be broken. In this situation, the band dispersion would be increasingly anisotropic, thus challenging one of the core principles of the PBA. A more accurate theoretical framework is therefore required to describe the measured PL spectra.

A. Spontaneous emission spectrum and eight-band *k.p* formalism

The spectrum r^{sp} is computed using the eight-band *k.p* formalism together with the EFA [41], following the simulation workflow summarized in Fig. 1. The eight-band *k.p* $Ge_{1-x}Sn_x$ material parametrization is based on early

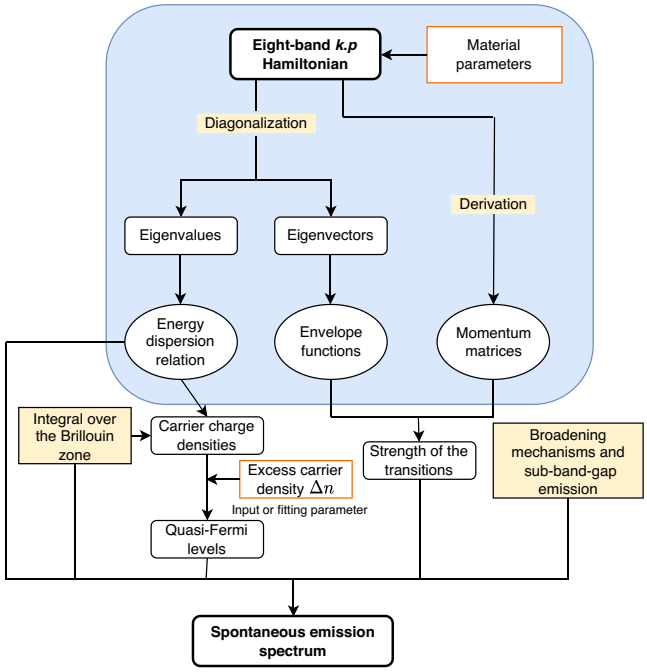

FIG. 1. Different steps followed in the computation of the spontaneous emission spectra.

reports [42–44], while strain implementation is based on the Bir-Pikus formalism [45]. To account for the inaccuracy of Vegard's law in estimating the band gaps of $Ge_{1-x}Sn_x$ alloys, band-gap bowing parameters are introduced for L and Γ high-symmetry points [42,46]. Unlike the JDOS model (and all the different models relying on the PBA), the evolution of the strength of the optical transitions, with the wave vector $\vec{k}$, is explicitly computed using the formalism developed by Szmulowicz [47]. This formalism requires accounting for the polarization of the incident light, and the derivative of the $k.p$ Hamiltonian with respect to the wave vector. The expressions of the different momentum matrices involved in the process can be found in the Supplemental Material S2 [48] (see also Refs. [26,27,47,49–55] therein).

For a given value of the optically injected carrier density Δn, if n_0 and p_0 denote the total electron and hole charge densities at thermal equilibrium, the quasi-Fermi levels μ_e (for electrons) and μ_h (for holes) are determined by solving the following set of equations:

$$\begin{aligned} n_0 + \Delta n &= \frac{1}{(2\pi)^3} \sum_{i\in \mathrm{CB}} \int_{\mathrm{BZ}} \frac{d^3\vec{k}}{1+\exp\left(\frac{\epsilon_i(\vec{k})-\mu_e}{kT}\right)}, \\ p_0 + \Delta n &= \frac{1}{(2\pi)^3} \sum_{i\in \mathrm{VB}} \int_{\mathrm{BZ}} \frac{d^3\vec{k}}{1+\exp\left(\frac{\mu_h-\epsilon_j(\vec{k})}{kT}\right)}. \end{aligned} \tag{4}$$

Herein, the conduction band electrons are assumed to be shared between the Γ and L valleys. This assumption is only relevant when the energy band offset between these valleys is relatively close to the thermal energy k_BT to enable the electrons to transition between them. When relevant, the electron density in the L valleys is computed with the PBA using the parameters given in Ref. [42]. The carrier concentrations n_0 and p_0 are evaluated after solving the electroneutrality equation to estimate the thermal equilibrium Fermi level E_F. Besides, the computation of the integrals over the BZ, required for estimating the quasi-Fermi levels and r^{sp}, relies on the special-lines approximation [56]. Within this approximation, the three-dimensional BZ integrals are replaced by a sum of one-dimensional integrals over some characteristic directions (denoted as "special") of the crystal lattice. These directions could, for example, be the symmetry directions used in the eight-band $k.p$ formalism. More information about all the different directions considered in our framework can be found in the Supplemental Material S3 [48].

Besides, to account for the sub-band-gap emission resulting from carrier disorders and broadening mechanisms in the materials, the initial definition of r^{sp}, presented in Refs. [26,27], is convoluted with a broadening function $\mathcal{B}$, which is usually chosen as a Gaussian or a Lorentzian to account for the inhomogeneous and homogeneous broadening mechanisms, respectively [57–59].

B. Spontaneous emission intensity and steady-state radiative carrier lifetime

The spontaneous emission rate R_{sp} is defined as the number of spontaneous recombinations per second in unit volume, and generally expressed by an integral [26]:

$$R_{\mathrm{sp}} = \int_0^{+\infty} r^{\mathrm{sp}}(\hbar\omega)\, d\hbar\omega. \tag{5}$$

This quantity makes it possible to estimate the steady-state radiative carrier lifetime τ_{rad}, which is defined by the density of photoexcited carriers Δn divided by the net spontaneous recombination rate $R_{\mathrm{sp}}^{\mathrm{net}}$. $R_{\mathrm{sp}}^{\mathrm{net}}$ designates the amount by which the nonequilibrium spontaneous recombination rate $R_{\mathrm{sp}}^{\mathrm{neq}}$ exceeds the thermal equilibrium spontaneous emission rate $R_{\mathrm{sp}}^{\mathrm{eq}}$ ($R_{\mathrm{sp}}^{\mathrm{net}} = R_{\mathrm{sp}}^{\mathrm{neq}} - R_{\mathrm{sp}}^{\mathrm{eq}}$). The net rate of spontaneous emission is usually characterized by a material-dependent parameter B known as the bimolecular, or radiative, recombination coefficient [Eq. (6)]:

$$R_{\mathrm{sp}}^{\mathrm{net}} = B(np - n_0p_0). \tag{6}$$

Also known as the capture probability, this variable is often used to estimate the efficiency of the material in terms of direct band-to-band radiative recombination. The bimolecular recombination coefficient B is typically assumed to be independent of Δn (and, therefore, of the quasi-Fermi levels). However, this approximation is not always accurate. For example, B was previously shown to vary linearly with

the excess carrier density Δn in III-V semiconductors [53–55]. In that case, rather than being a constant in Eq. (6), B is replaced by a new function $B(\Delta n)$, which can easily be computed from R_{sp}^{net}, derived using the $k.p$ formalism.

III. RESULTS AND DISCUSSION

The accuracy of the established theoretical framework has been evaluated through the analysis of the PL spectra recorded as a function of the excitation power and temperature from $Ge_{0.83}Sn_{0.17}$ layers [60]. The epitaxial growth of these layers is achieved using low-pressure chemical vapor deposition starting from a 600–700-nm Ge virtual substrate on a 4-inch Si wafer. To ensure the growth of a $Ge_{0.83}Sn_{0.17}$ layer with a uniform Sn composition, a multilayer heterostructure consisting of top layer/middle layer/bottom layer is grown while the incorporation of Sn in each layer is controlled by adjusting the growth temperature. More details of the growth and characterization of $Ge_{0.83}Sn_{0.17}$ material can be found in Ref. [60].

In as-grown $Ge_{0.83}Sn_{0.17}$ layers, the band alignment favors electron and hole diffusion to the top layer, where they should recombine. Indeed, the PL spectra are confirmed to originate from carrier recombination in this specific layer [60]. Therefore, from a theoretical standpoint, it would be judicious to analyze the PL results as if they were emitted by a bulk GeSn material with a 17 at. % Sn composition. On this basis, the different power-dependent PL spectra, recorded at 4 K, are fitted to the normalized calculated r^{sp} while using the excess carrier concentration Δn and γ the full width at half maximum of the broadening function as fitting parameters. This process allows the extraction of Δn and the quasi-Fermi levels, required to estimate the radiative carrier lifetime. Indeed, with μ_e and μ_h being the only missing parameters in the definition of r^{sp}, their extraction allows for the computation of the intensity R_{sp}^{net}, which is afterwards used to compute τ_{rad}. To solve Eq. (4), and extract the quasi-Fermi level couple (μ_e, μ_h), the p-type background doping is considered to be around 10^{15} cm^{-3} at 4 K. This value is chosen with reference to the p-type background doping estimated between 1×10^{17} and 5×10^{17} cm^{-3} at 300 K [10]. Besides, using the band-gap bowing parameter b_{GeSn}^{Γ} from Ref. [46], the direct-band-gap energy is expected to be 441 meV at 4 K. This value is higher than the peak position observed in PL spectra in the low-carrier-injection regime, thus standing in sharp contrast to what is expected from band-to-band spontaneous emission recombination [34]. To solve this issue, b_{GeSn}^{Γ} is adjusted by fitting the PL spectra in the low-carrier-injection regime, where the peak position is slightly above the direct-band-gap energy, following the same process as in Ref. [60], yielding a value of 2.674 eV at 4 K. The estimated direct-band-gap energy is subsequently used to fit the measured PL spectra at higher power densities. Using this value, the energy band offset between Γ and L valleys is found to be higher than 90 meV, thus making the electron population of the L valleys negligible.

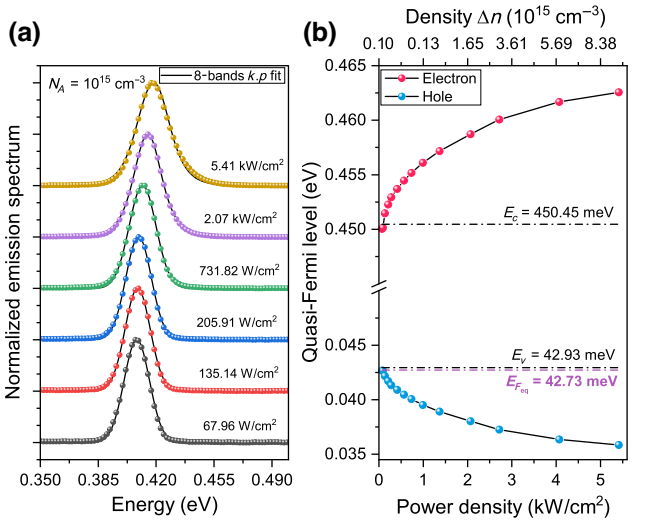

FIG. 2. (a) Power-dependent photoluminescence at 4 K for −1.3% biaxially strained $Ge_{0.83}Sn_{0.17}$. The scatter points are from the measurements while the black curves are the results from the simulations. (b) Evolution of the extracted quasi-Fermi levels (μ_e, μ_h) with the power density.

Figure 2(a) displays the measured and simulated spectra for the as-grown $Ge_{0.83}Sn_{0.17}$ material. For each power density, a coefficient of determination (R^2) of around 99.5% is obtained, thus highlighting the accuracy of the simulated spectra. Moreover, the evolution of the extracted quasi-Fermi levels with the excitation power density P_{exc} is outlined in Fig. 2(b).

For a p-type background doping of 10^{15} cm^{-3}, the thermal equilibrium the Fermi level E_F is about 42.73 meV. As shown in Fig. 2(b), the nondegenerate semiconductor approximation is not appropriate here since E_F is less than the top valence band edge located around 42.93 meV. Starting from a power density of 67.95 W/cm^2, both the electron and hole quasi-Fermi levels start to deviate from E_F. In fact, a progressive increase from 450.02 to 462.57 meV is observed for the quasi-Fermi level μ_e, causing the electron concentration to increase. Simultaneously, the hole quasi-Fermi level μ_h decreases while remaining very close to the thermal equilibrium level with a maximum offset of 6.88 meV at 5.4 kW/cm^2. While these variations may be perceived as small, they are not insignificant. Indeed, with a thermal energy of about 0.34 meV at 4 K, one should expect a noticeable increase in the spontaneous emission intensity R_{sp}. Moreover, the steady-state radiative carrier lifetime τ_{rad} is extracted [Fig. 3(a)] and shown to decrease from 3.52 to 1.89 ns in the range of power density used in this study.

Besides, the bimolecular recombination coefficient B is also evaluated using the different parameters obtained from

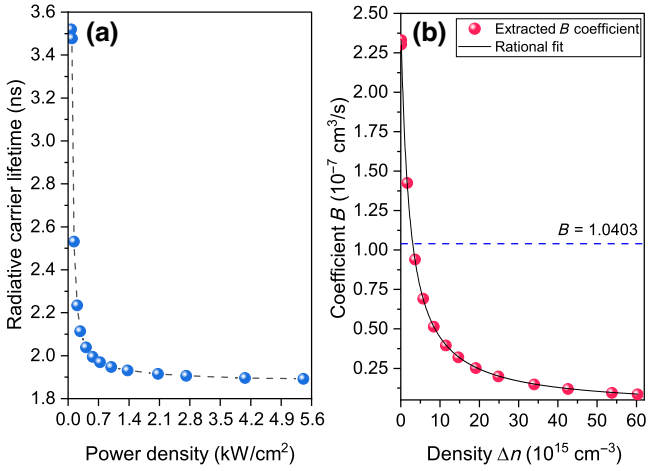

FIG. 3. (a) Evolution of the radiative carrier lifetime as a function of the excitation power density P_{exc}. (b) Evolution of the coefficient B as a function of the excess carrier density Δn. The filled circles represent the values of B computed from the extracted Δn, R_{sp} using Eq. (6), while the black curve is the result of a fit using a rational function.

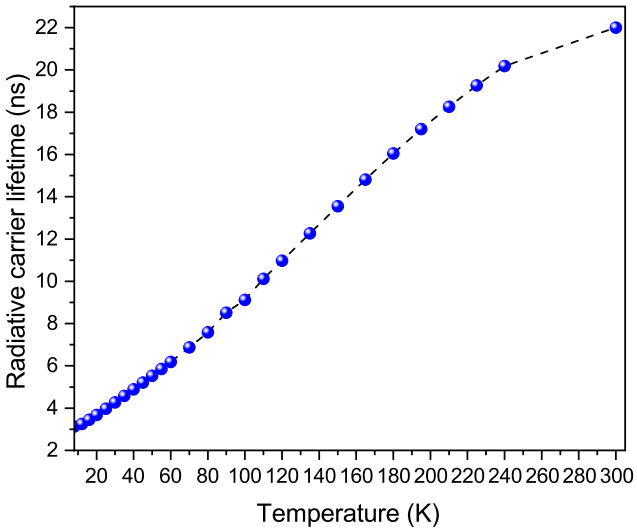

FIG. 4. Evolution of the radiative carrier lifetime as a function of temperature for the as-grown $Ge_{0.83}Sn_{0.17}$.

the analysis above, and its behavior is outlined in Fig. 3(b). Rather than being constant, it decreases with Δn, as suggested earlier for III-V semiconductors [53,54]. However, its evolution for the as-grown $Ge_{0.83}Sn_{0.17}$ is not as linear as presented by Olshansky *et al.* for In-Ga-As-P and Al-Ga-As light sources [55]. In fact, after performing a fit of the obtained data, B is shown to evolve with Δn following a rational function [Fig. 3(b)]. Additionally, for Δn above 10^{15} cm^{-3}, the values extracted are shown to be lower than the value of 1.04×10^{-7} cm^3/s computed assuming parabolic band dispersion and the nondegenerate semiconductor approximation (see Sec. S4 within the Supplemental Material for more details [48]).

The impact of temperature on the steady-state radiative carrier lifetime has also been investigated. Herein, assuming a p-type background doping of 1×10^{15} cm^{-3} at 4 K and 1×10^{17} cm^{-3} at 300 K, which is in line with recent measurements [10], the evolution of the doping with temperature is estimated. Using these values, the temperature-dependent PL spectra are fitted to the theoretical estimation of the spontaneous emission spectrum from the framework described above, and the evolution of τ_{rad} is extracted for the as-grown $Ge_{0.83}Sn_{0.17}$, as displayed in Fig. 4.

Note that from this analysis, a minimum R^2 factor of about 98% is observed throughout the range 4–300 K. The estimated steady-state radiative carrier lifetime τ_{rad} increases with the temperature from approximately 3.2 ns at 10 K to approximately 22.2 ns at 300 K. These values are very comparable to the reported recombination lifetimes in the literature for Ge and III-V compound semiconductors, which are generally in the nanoseconds range [61–64]. They are also of the same order of magnitude as the values reported for GeSn materials with Sn content below 10% [20]. However, it is important to note that the investigated layers in that work are highly compressively strained and thus of indirect band gap, whereas the current work addresses a material system that differs in defect density, Sn content, thickness, and band-gap directness. These parameters are expected to profoundly influence the radiative lifetime.

Finally, to appreciate the radiative emission strength of $Ge_{1-x}Sn_x$ with respect to other direct-band-gap semiconductors, we compare the radiative emission rate or more precisely the bimolecular recombination coefficient B. Using the same process as for the power-dependent PL, B is extracted as a function of the temperature. From this analysis, B is found to evolve following the allometric power law aT^b with $b \approx -1.5143$, and reaching 3.81×10^{-10} cm^3/s at 240 K. This value is comparable to those extracted at 300 K for Ga-As (3.5×10^{-10} cm^3/s), In-P (1.2×10^{-10} cm^3/s), and hexagonal $Si_{0.20}Ge_{0.80}$ (0.7×10^{-10}–11×10^{-10} cm^3/s).

IV. CONCLUSION

To circumvent the limitations in the experimental studies of carrier dynamics in narrow-band-gap $Ge_{1-x}Sn_x$ materials, this work demonstrates a straightforward method to obtain the carrier radiative lifetime from simple PL spectra. The approach relies on a theoretical framework combining band structure calculations using the $k.p$ formalism together with the envelope function approximation to estimate the absorption and spontaneous emission spectra. This framework simulates accurately the experimental measurements thereby allowing the evaluation of

the steady-state radiative carrier lifetime from the net rate of spontaneous emission and the density of photoexcited carriers. For a $Ge_{0.83}Sn_{0.17}$ material under an in-plane biaxial compressive strain $\varepsilon_{\parallel} = -1.3\%$, the analysis reveals a lifetime τ_{rad} in the nanosecond range increasing from 3 to 22 ns for temperatures between 10 and 300 K. Additionally, the introduced model also overcomes the restrictions that are inherent to the JDOS model resulting from the PBA and the weak-injection approximation.

ACKNOWLEDGMENTS

O.M. acknowledges support from NSERC Canada (Discovery, SPG, and CRD Grants), Canada Research Chairs, Canada Foundation for Innovation, Mitacs, PRIMA Québec, Defence Canada (Innovation for Defence Excellence and Security, IDEaS), the European Union's Horizon Europe research and innovation program under Grant No. 101070700 (MIRAQLS), and the U.S. Army Research Office (Grant No. W911NF-22-1-0277).

The authors declare no competing financial interest.

[1] O. Moutanabbir, S. Assali, X. Gong, E. O'Reilly, C. A. Broderick, B. Marzban, J. Witzens, W. Du, S.-Q. Yu, A. Chelnokov, D. Buca, and D. Nam, Monolithic infrared silicon photonics: The rise of (Si)GeSn semiconductors, Appl. Phys. Lett. **118**, 110502 (2021).

[2] D. Buca, A. Bjelajac, D. Spirito, O. Concepción, M. Gromovyi, E. Sakat, X. Lafosse, L. Ferlazzo, N. von den Driesch, Z. Ikonic, D. Grützmacher, G. Capellini, and M. El Kurdi, Room temperature lasing in GeSn microdisks enabled by strain engineering, Adv. Opt. Mater. **10**, 2201024 (2022).

[3] C.-Y. Chang, P.-L. Yeh, Y.-T. Jheng, L.-Y. Hsu, K.-C. Lee, H. Li, H. H. Cheng, and G.-E. Chang, Mid-infrared resonant light emission from GeSn resonant-cavity surface-emitting LEDs with a lateral p-i-n structure, Photonics Res. **10**, 2278 (2022).

[4] J. Chrétien, N. Pauc, F. Armand Pilon, M. Bertrand, Q.-M. Thai, L. Casiez, N. Bernier, H. Dansas, P. Gergaud, E. Delamadeleine, R. Khazaka, H. Sigg, J. Faist, A. Chelnokov, V. Reboud, J.-M. Hartmann, and V. Calvo, GeSn lasers covering a wide wavelength range thanks to uniaxial tensile strain, ACS Photonics **6**, 2462 (2019).

[5] J. Chrétien, Q. M. Thai, M. Frauenrath, L. Casiez, A. Chelnokov, V. Reboud, J. M. Hartmann, M. El Kurdi, N. Pauc, and V. Calvo, Room temperature optically pumped GeSn microdisk lasers, Appl. Phys. Lett. **120**, 051107 (2022).

[6] A. Elbaz, D. Buca, N. von den Driesch, K. Pantzas, G. Patriarche, N. Zerounian, E. Herth, X. Checoury, S. Sauvage, I. Sagnes, A. Foti, R. Ossikovski, J.-M. Hartmann, F. Boeuf, Z. Ikonic, P. Boucaud, D. Grützmacher, and M. El Kurdi, Ultra-low-threshold continuous-wave and pulsed lasing in tensile-strained GeSn alloys, Nat. Photonics **14**, 375 (2020).

[7] H.-J. Joo, Y. Kim, D. Burt, Y. Jung, L. Zhang, M. Chen, S. J. Parluhutan, D.-H. Kang, C. Lee, S. Assali, Z. Ikonic, O. Moutanabbir, Y.-H. Cho, C. S. Tan, and D. Nam, 1D photonic crystal direct bandgap GeSn-on-insulator laser, Appl. Phys. Lett. **119**, 201101 (2021).

[8] Y. Jung, D. Burt, L. Zhang, Y. Kim, H.-J. Joo, M. Chen, S. Assali, O. Moutanabbir, C. S. Tan, and D. Nam, Optically pumped low-threshold microdisk lasers on a GeSn-on-insulator substrate with reduced defect density, Photonics Res. **10**, 1332 (2022).

[9] X. Li, L. Peng, Z. Liu, Z. Zhou, J. Zheng, C. Xue, Y. Zuo, B. Chen, and B. Cheng, 30 GHz GeSn photodetector on SOI substrate for 2μm wavelength application, Photonics Res. **9**, 494 (2021).

[10] M. R. M. Atalla, S. Assali, A. Attiaoui, C. Lemieux-Leduc, A. Kumar, S. Abdi, and O. Moutanabbir, All-group IV transferable membrane mid-infrared photodetectors, Adv. Funct. Mater. **31**, 2006329 (2021).

[11] X. Liu, J. Zheng, C. Niu, T. Liu, Q. Huang, M. Li, D. Zhang, Y. Pang, Z. Liu, Y. Zuo, and B. Cheng, Sn content gradient GeSn with strain controlled for high performance GeSn mid-infrared photodetectors, Photonics Res. **10**, 1567 (2022).

[12] L. Luo, S. Assali, M. R. M. Atalla, S. Koelling, A. Attiaoui, G. Daligou, S. Martí, J. Arbiol, and O. Moutanabbir, Extended-SWIR photodetection in all-group IV core/shell nanowires, ACS Photonics **9**, 914 (2022).

[13] B. Marzban, L. Seidel, T. Liu, K. Wu, V. Kiyek, M. H. Zoellner, Z. Ikonic, J. Schulze, D. Grützmacher, G. Capellini, M. Oehme, J. Witzens, and D. Buca, Strain engineered electrically pumped SiGeSn microring lasers on Si, ACS Photonics **10**, 217 (2023).

[14] E. Talamas Simola, V. Kiyek, A. Ballabio, V. Schlykow, J. Frigerio, C. Zucchetti, A. De Iacovo, L. Colace, Y. Yamamoto, G. Capellini, D. Grützmacher, D. Buca, and G. Isella, CMOS-compatible bias-tunable dual-band detector based on GeSn/Ge/Si coupled photodiodes, ACS Photonics **8**, 2166 (2021).

[15] H. Tran, T. Pham, J. Margetis, Y. Zhou, W. Dou, P. C. Grant, J. M. Grant, S. Al-Kabi, G. Sun, R. A. Soref, J. Tolle, Y.-H. Zhang, W. Du, B. Li, M. Mortazavi, and S.-Q. Yu, Si-based GeSn photodetectors toward mid-infrared imaging applications, ACS Photonics **6**, 2807 (2019).

[16] S. Xu, W. Wang, Y.-C. Huang, Y. Dong, S. Masudy-Panah, H. Wang, X. Gong, and Y.-C. Yeo, High-speed photo detection at two-micron-wavelength: Technology enablement by GeSn/Ge multiple-quantum-well photodiode on 300 mm Si substrate, Opt. Express **27**, 5798 (2019).

[17] Y. Zhou, Y. Miao, S. Ojo, H. Tran, G. Abernathy, J. M. Grant, S. Amoah, G. Salamo, W. Du, J. Liu, J. Margetis, J. Tolle, Y.-h. Zhang, G. Sun, R. A. Soref, B. Li, and S.-Q. Yu, Electrically injected GeSn lasers on Si operating up to 100 K, Optica **7**, 924 (2020).

[18] M. R. M. Atalla, S. Assali, S. Koelling, A. Attiaoui, and O. Moutanabbir, High-bandwidth extended-SWIR GeSn photodetectors on silicon achieving ultrafast broadband spectroscopic response, ACS Photonics **9**, 1425 (2022).

[19] B. Julsgaard, N. von den Driesch, P. Tidemand-Lichtenberg, C. Pedersen, Z. Ikonic, and D. Buca, Carrier lifetime of GeSn measured by spectrally resolved picosecond photoluminescence spectroscopy, Photon. Res. **8**, 788 (2020).

[20] E. Vitiello, S. Rossi, C. A. Broderick, G. Gravina, A. Balocchi, X. Marie, E. P. O'Reilly, M. Myronov, and F. Pezzoli, Continuous-wave magneto-optical determination of the carrier lifetime in coherent $Ge_{1-x}Sn_x/ge$ heterostructures, Phys. Rev. Appl. **14**, 064068 (2020).

[21] M. K. Hudait, S. W. Johnston, M. B. Clavel, S. Bhattacharya, S. Karthikeyan, and R. Joshi, High carrier lifetimes in epitaxial germanium–tin/Al(In)As heterostructures with variable tin compositions, J. Mater. Chem. C **10**, 10530 (2022).

[22] B. E. A. Saleh and M. C. Teich, *Fundamentals of Photonics, 2 Volume Set: 2 Volume Set* (John Wiley & Sons, Nashville, TN, 2019), 3rd ed.

[23] G. Lasher and F. Stern, Spontaneous and stimulated recombination radiation in semiconductors, Phys. Rev. **133**, A553 (1964).

[24] P. Wurfel, The chemical potential of radiation, J. Phys. C: Solid State Phys. **15**, 3967 (1982).

[25] J. K. Katahara and H. W. Hillhouse, Quasi-Fermi level splitting and sub-bandgap absorptivity from semiconductor photoluminescence, J. Appl. Phys. **116**, 173504 (2014).

[26] S. L. Chuang, *Physics of Photonic Devices*, Wiley Series in Pure and Applied Optics (Wiley-Blackwell, Hoboken, NJ, 2008), 2nd ed.

[27] P. T. Landsberg, *Recombination in Semiconductors* (Cambridge University Press, Cambridge, England, 1992), 1st ed.

[28] H. Wen and E. Bellotti, Rigorous theory of the radiative and gain characteristics of silicon and germanium lasing media, Phys. Rev. B **91**, 035307 (2015).

[29] H. Wen, B. Pinkie, and E. Bellotti, Direct and phonon-assisted indirect Auger and radiative recombination lifetime in HgCdTe, InAsSb, and InGaAs computed using Green's function formalism, J. Appl. Phys. **118**, 015702 (2015).

[30] S. Dominici, H. Wen, F. Bertazzi, M. Goano, and E. Bellotti, Numerical study on the optical and carrier recombination processes in GeSn alloy for E-SWIR and MWIR optoelectronic applications, Opt. Express **24**, 26363 (2016).

[31] G. Pizzi, M. Virgilio, and G. Grosso, Tight-binding calculation of optical gain in tensile strained [001]-Ge/SiGe quantum wells, Nanotechnology **21**, 055202 (2009).

[32] D. J. Paul, 8-band $k\cdot$ modelling of mid-infrared intersubband absorption in Ge quantum wells, J. Appl. Phys. **120**, 043103 (2016).

[33] C. Grein, M. Flatté, and Y. Chang, Modeling of recombination in HgCdTe, J. Electron. Mater. **37**, 1415 (2008).

[34] E. F. Schubert, *Light-Emitting Diodes* (Cambridge University Press, Cambridge, England, 2012), 2nd ed.

[35] D.-L. Zhang, B.-W. Cheng, C.-L. Xue, X. Zhang, H. Cong, Z. Liu, G.-Z. Zhang, and Q.-M. Wang, Theoretical study of the optical gain characteristics of a $Ge_{1-x}Sn_x$ alloy for a short-wave infrared laser, Chinese Physics B **24**, 024211 (2015).

[36] D. Stange, *Group IV (Si)GeSn light emission and lasing studies*, Dissertation, RWTH Aachen University, Jülich (2019), druckausgabe: 2019. - Onlineausgabe: 2019. - Auch veröffentlicht auf dem Publikationsserver der RWTH Aachen University; Dissertation, RWTH Aachen University, 2019.

[37] S. Wirths, *Group IV epitaxy for advanced nano- and optoelectronic applications*, Dissertation, RWTH Aachen, Jülich (2016), druckausgabe: 2016. - Onlineausgabe: 2016. - Auch veröffentlicht auf dem Publikationsserver der RWTH Aachen University; Dissertation, RWTH Aachen, 2015.

[38] H.-L. Chen, C. Himwas, A. Scaccabarozzi, P. Rale, F. Oehler, A. Lemaître, L. Lombez, J.-F. Guillemoles, M. Tchernycheva, J.-C. Harmand, A. Cattoni, and S. Collin, Determination of *n*-type doping level in single GaAs nanowires by cathodoluminescence, Nano Lett. **17**, 6667 (2017), pMID: 29035545.

[39] E. M. T. Fadaly, A. Dijkstra, J. R. Suckert, D. Ziss, M. A. J. van Tilburg, C. Mao, Y. Ren, V. T. van Lange, K. Korzun, S. Kölling, M. A. Verheijen, D. Busse, C. Rödl, J. Furthmüller, F. Bechstedt, J. Stangl, J. J. Finley, S. Botti, J. E. M. Haverkort, and E. P. A. M. Bakkers, Direct-bandgap emission from hexagonal Ge and SiGe alloys, Nature **580**, 205 (2020).

[40] A. Dijkstra, *Optical properties of direct band gap group IV semiconductors*, Ph.D. thesis, Applied Physics and Science Education (2021), proefschrift. - Embargo 1 year, pdf open access 28-5-2022.

[41] T. B. Bahder, Eight-band $\mathbf{k}\cdot\mathbf{p}$ model of strained zinc-blende crystals, Phys. Rev. B **41**, 11992 (1990).

[42] G.-E. Chang, S.-W. Chang, and S. L. Chuang, Strain-balanced $Ge_zSn_{1-z} - Si_xGe_ySn_{1-x-y}$ multiple-quantum-well lasers, IEEE J. Quantum Electron. **46**, 1813 (2010).

[43] K. Lu Low, Y. Yang, G. Han, W. Fan, and Y.-C. Yeo, Electronic band structure and effective mass parameters of $Ge_{1-x}Sn_x$ alloys, J. Appl. Phys. **112**, 103715 (2012).

[44] M. P. Polak, P. Scharoch, and R. Kudrawiec, The electronic band structure of $Ge_{1-x}Sn_x$ in the full composition range: Indirect, direct, and inverted gaps regimes, band offsets, and the Burstein–Moss effect, J. Phys. D: Appl. Phys. **50**, 195103 (2017).

[45] G. L. Bir and G. E. Pikus, *Symmetry and Strain-Induced Effects in Semiconductors* (Wiley, New York, 1974).

[46] M. Bertrand, Q.-M. Thai, J. Chrétien, N. Pauc, J. Aubin, L. Milord, A. Gassenq, J.-M. Hartmann, A. Chelnokov, V. Calvo, and V. Reboud, Experimental calibration of Sn-related Varshni parameters for high Sn content GeSn layers, Ann. Phys. **531**, 1800396 (2019).

[47] F. Szmulowicz, Derivation of a general expression for the momentum matrix elements within the envelope-function approximation, Phys. Rev. B **51**, 1613 (1995).

[48] See Supplemental Material at http://link.aps.org/supplemental/10.1103/PhysRevApplied.20.064001 for more details about the momentum matrix elements and the special points approximation, which includes Refs. [26,27,47,49–55].

[49] S. Birner, *Modeling of Semiconductor Nanostructures and Semiconductor-Electrolyte Interfaces*, 1st ed., Selected Topics of Semiconductor Physics and Technology No. Vol. 135 (Verein zur Förderung des Walter Schottky Instituts der Technischen Universität München, 2011).

[50] T. Eißfeller, *Theory of the Electronic Structure of Quantum Dots in External Fields*, 1st ed., Selected Topics of Semiconductor Physics and Technology No. Vol. 146 (Verein

zur Förderung des Walter-Schottky-Inst. der Techn. Univ. München, 2012).

[51] E. Kane, Energy band structure in p-type germanium and silicon, J. Phys. Chem. Solids **1**, 82 (1956).

[52] P. Enders, Addendum to "Special-lines approximation to Brillouin zone integration": Improved set of special lines, Semicond. Sci. Technol. **11**, 1927 (1996).

[53] F. Stern, Calculated spectral dependence of gain in excited GaAs, J. Appl. Phys. **47**, 5382 (1976).

[54] C. B. Su, R. Olshansky, J. Manning, and W. Powazinik, Carrier dependence of the radiative coefficient in III-V semiconductor light sources, Appl. Phys. Lett. **44**, 732 (1984).

[55] R. Olshansky, C. Su, J. Manning, and W. Powazinik, Measurement of radiative and nonradiative recombination rates in InGaAsP and AlGaAs light sources, IEEE J. Quantum Electron. **20**, 838 (1984).

[56] P. Enders, Special-lines approximation to Brillouin zone integration, Semicond. Sci. Technol. **11**, 187 (1996).

[57] E. F. Schubert, E. O. Göbel, Y. Horikoshi, K. Ploog, and H. J. Queisser, Alloy broadening in photoluminescence spectra of $Al_xGa_{1-x}As$, Phys. Rev. B **30**, 813 (1984).

[58] D. Ouadjaout and Y. Marfaing, Localized excitons in II-VI semiconductor alloys: Density-of-states model and photoluminescence line-shape analysis, Phys. Rev. B **41**, 12096 (1990).

[59] M. Asada, Intraband relaxation time in quantum-well lasers, IEEE J. Quantum Electron. **25**, 2019 (1989).

[60] S. Assali, A. Dijkstra, A. Attiaoui, E. Bouthillier, J. Haverkort, and O. Moutanabbir, Midinfrared emission and absorption in strained and relaxed direct-band-gap Ge_{1-x} Sn_x semiconductors, Phys. Rev. Appl. **15**, 024031 (2021).

[61] J. Feldmann, G. Peter, E. O. Göbel, P. Dawson, K. Moore, C. Foxon, and R. J. Elliott, Linewidth dependence of radiative exciton lifetimes in quantum wells, Phys. Rev. Lett. **59**, 2337 (1987).

[62] J. Bellessa, V. Voliotis, R. Grousson, X. L. Wang, M. Ogura, and H. Matsuhata, Quantum-size effects on radiative lifetimes and relaxation of excitons in semiconductor nanostructures, Phys. Rev. B **58**, 9933 (1998).

[63] G. 't Hooft, M. Leys, and H. Talen-v.d. Mheen, Temperature dependence of the radiative recombination coefficient in GaAs-(Al, Ga)As quantum wells, Superlattices Microstruct. **1**, 307 (1985).

[64] C. Rödl, J. Furthmüller, J. R. Suckert, V. Armuzza, F. Bechstedt, and S. Botti, Accurate electronic and optical properties of hexagonal germanium for optoelectronic applications, Phys. Rev. Mater. **3**, 034602 (2019).